IIETA International Information and Engineering Technology Association
Advancing the World of Information and Engineering

Annales de Chimie - Science des Matériaux
Vol. 46, No. 4, August, 2022, pp. 173-183
Journal homepage: http://iieta.org/journals/acsm

Corroded RC Beam Behavior Subjected to Random Loading in Various Pore Saturation Levels: Coupled Numerical Analysis

Yasmine Meterfi[1*], Habib Trouzine[1], Youcef Houmadi[2]

[1] Civil Engineering and Environmental Laboratory, Department of Civil Engineering and Public Works, Faculty of Technology, Sidi Bel Abbes University, DZ 22000, Algeria
[2] Smart Structures Laboratory, Ain Témouchent University, DZ 46000, Algeria

Corresponding Author Email: yasmine.meterfi@univ-sba.dz

https://doi.org/10.18280/acsm.460402

Received: 31 May 2022
Accepted: 23 July 2022

Keywords:
concrete, corrosion, infrastructures, modeling, coupling techniques, pore saturation

ABSTRACT

Steel represents the majority of civil infrastructure. Corrosion is the principal source of structural degradation, primarily affected by the aggressive environment corrosion is a multiphysical process that occurs at the steel/electrolyte interface. This work presents a mechano-electrochemical coupling study of a corroded reinforced concrete (RC) beam subjected to section loss and a randomly varying load over time. A corrosion cell is created by connecting a zinc anode electrically to the RC beam system. This study uses numerical coupling techniques based on the mechanistic and kinetics of the corrosion process to evaluate the corrosion rate at different pore saturation degrees. The results reveal the impact of section loss on the RC beam displacement over time; as the cross-section reduces, the beam's ductility decreases, resulting in a yield and ultimate strength reduction. The moisture content effect on the electrochemical corrosion processes and oxygen diffusivity indicate that pore saturation levels are the primary determinant of the corrosion rate. The proposed numerical model explains the efficiency of coupled numerical analysis in the RC beam mechanical behavior assessment under corrosive conditions; the results include the concrete's porosity impact on the electrochemical corrosion process and the zinc anode contribution to steel corrosion protection.

1. INTRODUCTION

Corrosion is a complex spontaneous degradation process that can be chemical or electrochemical, caused by interactions with the surrounding environment. Infrastructures can be exposed to various environmental and climatic shifting conditions, which increase their vulnerability to several types of corrosion. Hot gas aggressions engender high-temperature corrosion, whereas aqueous corrosion results from aqueous electrolytes and structural interactions [1].

Under natural atmospheric conditions, the concrete tends to carbonize, resulting in steel reinforcement corrosion, affecting structural performance by limiting the concrete's functional durability [2].

The infrastructures' durability and behavior under changing climatic conditions are significantly affected by multiple factors. These factors can be mechanical (seismic, vibration, overloading), physical (fire, snow, frost), chemical (chloride, soil chemicals), or biological (plants, microorganisms). Mechanical factors are included in structural analysis in concrete structures' durability assessment. However, the ingress of aggressive chemical substances through the concrete, porous network requires further investigations [3].

During any construction, concrete undergoes cracking due to internal and external stresses, temperature variation, shrinkage, fatigue loads, and excess water in the mix. As the concrete is reinforced with steel bars to strengthen the tensile zone, the cracks do not only affect the concrete's durability. Still, they will facilitate the penetration of gases, liquids, and aggressive chemical substances throughout the concrete bulk targeting the reinforcement and causing corrosion [4].

Corrosion in civil infrastructures is principally induced by environmental factors such as penetration of chlorides or carbonation. These factors are generally influenced by climatic parameters like (CO_2, relative humidity, temperature, chloride's coefficient of diffusion, chloride's concentration boundary, etc...), concrete properties, and materials' chemical and mechanical composition.

As heterogeneous environments, soils are the site of the most complex corrosion mechanisms, making soil corrosion the major problem affecting infrastructures.

The behavior of geotechnical structures is a soil-structure interaction problem [5]. Steel-electrolyte interactions depend mainly on contributing factors such as the electrolyte properties, electrolyte nature (steel-soil, steel-concrete, steel-seawater, etc.), as well as the used materials in the structure construction process, the dimension of the structural elements, and the type of applied loads.

Recently, a significant effort and various approaches have been invested into computing technologies and calculation methodologies. The interpretation of the corrosions complex process requires realistic simulations and detailed numerical models.

Numerical modeling is a fundamental tool in identifying complex phenomena threatening the infrastructures' durability [6].

Modeling and simulation are gaining insight into durability assessment and materials behavior analyses under various

conditions.

In the literature, the prediction of corrosion has been carried out using two approaches: deterministic models based on numerical calculations and stochastic probabilistic models. According to Fujimoto [7], the stochastic and probabilistic approaches may not always be efficient with new materials composition and unpredictable environmental conditions, which require deterministic models. In recent technical advances, numerical calculations are based principally on finite element methods (FEM); the development of reliable numerical models and simulations such as finite element analysis is fundamental in future predictive maintenance concepts [8]. The development and improvement of numerical tools simplified the computations by integrating multiple modules and different features in the FEM software, such as electrochemistry, using shapes, boundary conditions, and site conditions, which improve the analysis and assessment of various types of corrosion complex process [9, 10].

The multiphysics aspect of the corrosion process requires interdisciplinary methodologies combining multiple approaches with diverse engineering expertise that involves coupling techniques to simulate the different connected phenomena [11].

The corrosion process is a surface phenomenon, and it's described as the interconnection of the different separate components of the involved chemical reactions and the manifestation of the heterogeneous mechanical actions on these chemical reactions [12].

The corrosion mechanisms can be caused or accelerated by mechanical actions; the mechano-electrochemical effect is the interaction between the corrosion electrochemical reactivity on a steel surface and the internal or external applied stress on that surface layer [13].

Infrastructure elements undergo frequent external forces, multiple types of strains, mechanical stresses, and the influence of the initial state of the soil pressure. Combining these factors can cause critical degradation that leads to unpredictable accidents [14]. Local stress and factors that increase strain, such as corrosion defects and mechanical cracks, are current on the infrastructure's surface as irregularities that cause local plastic deformation [15].

Numerous researches demonstrate that the corrosion's chemical reactions on the steel would slightly increase under external stress. The local corrosion behavior augments significantly when the applied tensile strain or the geometry of the corrosion defect is sufficient to induce plastic deformation. The mechano-electrochemical effect on stressed steel becomes critical in the plastic phase of deformation [16, 17]; a complete analysis of the corroded system's mechanical behavior and its interactions with the surrounding environment is a fundamental step in the infrastructure's durability assessment.

The general degradation rate of infrastructures is primarily governed by the corrosion rate, which determines the structure's deterioration process [18].

The steel corrosion rate evaluation is crucial in the residual load-bearing capacity analysis of the structural elements to quantify the actual degree of the structure's damage and predict the degradation evolution during the infrastructure's service life [18].

Analytical approaches are limited in estimating corrosion rates; therefore, numerical techniques are commonly used in the assessment of steel surface's state under multiple conditions by using numerical models to numerically calculate the corrosion rates, including oxygen diffusion, cathodic/anodic reactions, active-passive transitions, and oxide layer formation, by solving the related physicochemical and electrochemical equations in space and time domains [19].

To have an indicative value of the corrosion current, Andrade and Alonso [18] developed a model providing a framework for the correct measurement of corrosion rates, including the variability of weather conditions and climatic parameters that influence the moisture content of the concrete.

Muehlenkamp et al. [20] investigated the corrosion rate for various moisture contents of concrete; the study revealed that the transport properties for ions and gases vary with the concrete's moisture content, which significantly impacts the corrosion current densities rate. Jašniok and Jašniok [21] affirmed that the effect of the changing climatic conditions on corrosion rate depends on temperature variations, while moisture content in concrete has no significant impact on corrosion rate and is unaffected by humidity. Chen and Su [22] implemented the polarization resistance method (PRM) to microcell and macrocell corrosion (MMC) of reinforced concrete, as the PRM can precisely compute the corrosion current density due to its direct and quick performance and accuracy. Within a deterministic context. Nasser et al. [23] used the damage relations founded on visual surveys to investigate the efficiency of a structured 2D model in predicting the behavior of corroded reinforced concert beams.

Numerous ongoing research on the interaction between moisture content and the average corrosion rate are conducted in the literature; Azoor et al. [24] worked on the existence of the optimum moisture level, the level that leads to a high corrosion rate in various soils with different degrees of saturation. Their study revealed that each soil has an optimum saturation degree at which the corrosion rate is maximized and that the soil-metal interface is affected by soil structure, moisture distribution, and oxygen diffusion that directly influences underground corrosion. Hirata et al. [25] studied the corrosion behavior of carbon steel in artificial soils with varying saturation degrees; the results pointed out that the carbon steel corroded uniformly slower in saturated soil and non-uniformly faster in unsaturated soil.

The beam is a mechanical system that can be a real topic that simplifies the demonstration of the coupling numerical approach's adaptability. In the present study, an RC beam model is used to illustrate the applicability of the coupled numerical techniques in the RC beam mechanical behavior assessment in corrosion conditions. The steel part of the RC beam model serving as the framework of this study is derived from reference [26]. Andrieu-Renaud et al. [26] used this bending steel beam model to compute the probability of failure using a method called PHI2 that allows for solving time-variant reliability problems employing classical time-invariant reliability tools such as the First and second-order reliability methods FORM/SORM.

The present work demonstrates the efficiency of mechano-electrochemical coupling techniques in analyzing the behavior of a corroded RC beam under a random variable load during the complex corrosion process. The simulation is run for various pore saturation levels to evaluate the impact of the moisture content on the corrosion mechanism.

The applied load values vary randomly to consider environmental changes such as (wind speed, temperature, wave height, occupancy loads, transport loads, etc.) in the practical durability assessment.

The study aims to assess the corrosion rate evolution of an RC beam under time-dependent varying loads for various pore

saturation degrees in a simulated concrete pore solution by including the oxygen diffusion and the mechanical impact of the time-dependent stress on the corroded element.

The results showed the critical impact of corrosion on the total displacement, affecting the corroded steel element ductility. The role of the pore saturation degree of the simulated concrete in governing the corrosion rate is also demonstrated, confirming the impact of pore saturation on oxygen mass transport resistance.

The corrosion rate and the corroded RC beam behavior are evaluated using numerical analysis by coupling numerical modeling techniques. The zinc anode's impact on the corrosion rate and the steel protection is also highlighted in this work, proving the efficiency of the implemented zinc anode in corrosion protection.

This paper is structured as follows: previous studies related to this work are summarized in the literature review section. The material and method section is divided into two parts: the first part considers the mechanical behavior of the steel under isotropic corrosion evolving linearly over time. Corrosion rates at various pore saturation degrees are investigated in the second part. The finding illustration is detailed in the results and discussion section, finishing with a conclusion synthesizing the aims and importance of the work's findings and the interest, in using the coupled numerical method in assessing RC elements.

2. LITERATURE REVIEW

Multiple studies evaluating the interaction between moisture content and the average corrosion rate are conducted, to investigate the corrosion rates in various electrolytes such as soil, concrete, and seawater.

Muehlenkamp et al. [20] investigated the corrosion rate for different moisture contents of concrete by developing a numerical model for the cathodic protection of steel embedded in concrete. The diffusion of oxygen and the charge conduction parameters are considered in the study as a function of concrete moisture content. Their study revealed that corrosion current densities are higher for low pore saturation levels. The transport properties for ions and gases vary with the concrete's moisture content as concrete is a porous material, which significantly impacts the corrosion current densities rate. Jašniok and Jašniok [21] demonstrated that the influence of climatic change conditions on corrosion rate is based on the change of temperature by conducting electrochemical tests under different temperature and humidity conditions. Their analysis showed that the effect of the changing climatic conditions on corrosion rate depends on temperature variations, while moisture content in concrete has no significant impact on changes in corrosion rate and does not depend on humidity. The interface soil-metal is dependent on the soil structure and moisture distribution as well as the oxygen diffusion that directly influences the soil corrosion; Azoor et al. [24] investigated the corrosion rates in different soils, revealing that each soil has optimum degrees of saturation at which the corrosion rate is maximized. Hirata et al. [25] used artificial soils to investigate the corrosion behavior of carbon steel in varying saturation degrees; Their study revealed that the corrosion evolves uniformly slower in saturated soil and non-uniformly faster in unsaturated soil. To have a representative value of the corrosion current, Andrade and Alonso [18] developed a model to present the basis for the correct measurement of the corrosion rate in their work, including the variability of weather conditions and climatic parameters that influence the moisture content of the concrete in the estimation of polarization resistance. Linares-Alemparte et al. [3] investigated the oxygen diffusion in concrete analytically, including the oxygen diffusion coefficient, concrete porosity, and electrical resistivity measurements. The results revealed the relevant link between porosity diffusion coefficient and electrical resistivity.

Various external forces and factors affect the corrosion rate and the mechanical response of the structure's corroded parts. To quantify the influence of corrosion width, depth, and length, Li et al. [14] studied the impact of those factors on the dynamic response of concrete pipelines under the coupled effect of earth pressure and traffic load, implementing parametric and sensitivity analysis to estimate the parameter sensitivity by evaluating the influence of the corrosion depth, width, and length on the model output. Xu and Cheng [27] demonstrated the critical impact of the mechano-electrochemical effect on the corrosion defects growth using a finite element model, including time dependency in determining the corrosion reaction and the defect geometry. Their study revealed that the mechano-electrochemical effect accelerates the localized corrosion with time due to the rapid increase in the stress concentration and anodic current density at the defect. They've also highlighted the impact of cathodic protection in reducing the speed growth of corrosion defects. Khemissa et al. [5] used numerical simulation employing elastoplastic models to study the behavior of the sand-steel interface under monotonic loading. The results show the soil–structure interface and geotechnical structure interactions as well as the influence of interface roughness and the structure constituting materials in determining the shear strength parameter characteristics of the sand–steel interface. Bogdanov et al. [13] summarized the findings of the mechanochemical and chemomechanical surface effects under the simultaneous effects of stresses/strains and corrosion in their work, including the mechanism and kinetics of corrosion cracking. The literature analysis has shown that all authors agreed that the corrosion defects growth, and the cracks propagation, are accelerated by the mechanochemical effect that speeds up the anodic dissolution under an applied load. Chen et al. [28] worked on non-uniform corrosion of steel bars in concrete, including time dependency at different locations using a numerical model. The oxygen diffusion and chloride penetration under longitudinal defects are also evaluated. The result demonstrates the impact of corrosion-induced cracking on increasing the chloride penetration and oxygen diffusion, accelerating the steel-rebar corrosion. Nasser et al. [23] used the damage relations based on visual inspection data to study the efficiency of a 2D modeling approach in predicting the behavior of corroded reinforced concert beams. Kabashi et al. [29] worked on a comparative approach of a reinforced beam flexural behavior with steel bars and fiber reinforced polymers, considering corrosion in aggressive environmental conditions. Wang et al. [30] studied the corrosion mechanism in multi-physics coupled environments, including time dependency, electrode reaction kinetics, mass transfer, and ion concentration, revealing the impact of the combined effect of the solution chemistry and electrical field on the corrosion process. Yu et al. [31] studied corrosion under structural defects and the non-uniformity of material deterioration using a combined method including electrochemical and chemo-physical-mechanical models. The result underlines the

importance of integrating material non-uniformity as the non-uniform distributions of porosity, oxygen content, and oxygen diffusivity into an electrochemical model to estimate the distributions of potential fields and current density.

Goyal et al. [32] evaluated the protection current and potential distribution over variant reinforcement layers in concrete. A parametric study is employed in their work to investigate the concrete resistivity and applied current density impact on protection. The dependence of protection on concrete resistivity is demonstrated.

The present study uses an RC beam 3D model to illustrate the applicability of the coupled numerical techniques in the RC beam mechanical behavior assessment under corrosion conditions. This work combines the mechano-electro-chemical effect on the corrosion rate evolution under varying loads for various pore saturation degrees in a simulated concrete. The analysis includes the oxygen diffusion in the different pore saturation levels and the mechanical impact of the time-dependent stress on the behavior of the corroded element. The steel protection is also highlighted in this work, proving the efficiency of the implemented zinc anode in corrosion protection and its impact on the corrosion rate.

3. MATERIAL AND METHODS

The choice of the RC bending beam model (Figure 1) is based on its simple geometry and the properties of the used materials that facilitate the modeling and implementation of this mechanical system in numerical analysis.

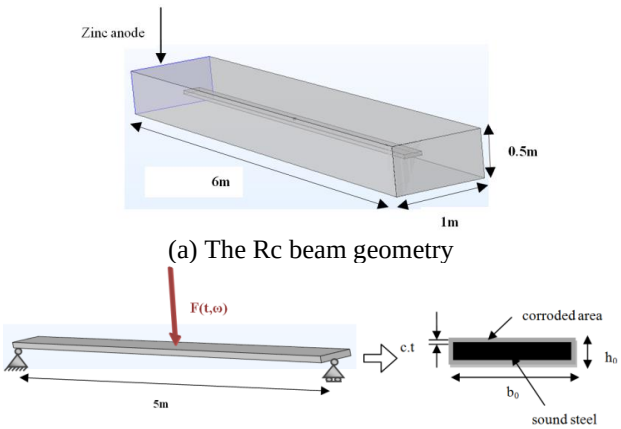

(a) The Rc beam geometry

(b) The corroded steel geometry

Figure 1. The corroded bending RC beam 3Dmodel

The present study is conducted employing a numerical simulation. The work process is organized as follows: the study is divided into two parts: the first part focuses on the beam behavior under uniform corrosion submitted to varying applied stresses. To better understand the impact of the sectional loss due to corrosion on the beam behavior, the mechanical study in the first part is conducted only on the steel part of the beam Figure 1 (b), the steel model geometry is derived from the study [26], the considered degradation mechanism is the reduction of the steel section due to corrosion process.

A stochastic process is used to define the behavior of the considered load, which varies randomly over time following a normal distribution. The second part includes the simulated concrete electrolyte in the analysis, considering the entire RC beam system. The corrosion rate is evaluated at diverse concrete moisture levels (i.e., at different pore saturation degrees). The impact of the added zinc anode position on the corrosion rate along the steel interface is underlined, demonstrating the efficiency of the implemented anode in the steel surface corrosion protection.

Due to data insufficiency, the simulated concrete properties and the modeling conditions parameters are derived from the work of Muehlenkamp et al. [20], which focuses on the prediction of spatial uniformity of the steel's cathodic protection in concrete under the moisture's impact, using a two-dimensional cross-section of a reinforced concrete's repeating unit.

3.1 Part one

Figure 1 (a) illustrates the simply supported bending RC beam with the following parameters:

The length (L=6 m), the width (B=1 m), the height (H=0.5 m).

As mentioned before, the mechanical study is conducted on the corroded steel part of the RC beam Figure 1 (b), with the following parameters derived from [26]:

The length (L=5 m), a rectangular cross-section area (b_0=0.2 m, h_0=0.04 m), b_0, and h_0 are the initial dimensions of the cross-section (before corrosion).

Isotropic corrosion evolving linearly over time attacks all segments of the steel beam surface.

The beam is subjected to its own weight (body load) $W=\rho_{st}b_0h_0$ (N/m) represented by a uniformly distributed load where the steel density ρ_{st} = 78500 N/m^3, and also a concentrated force F applied at mid-span (see Figure 1 (a)).

The corrosion starts at t=0, increases linearly in time between t_i=0 and t_f=10 years with a corrosion coefficient c=0.05mm/year.

The load is considered as a variable over time, represented by F(t), a stationary process following a stochastic gaussian(normal) distribution with the parameters: Mean μ=5800N, Standard deviation σ=1160N, and an exponential square autocorrelation coefficient function:

$$\exp\left(\left(\frac{\Delta_t}{l}\right)^2\right) \quad (1)$$

The correlation length l =1 year.

A load vector containing 41 random values is generated using the cited parameters.

The time interval is discretized into 41 instants. The time discretization step Δt= 3 months ↔ 0.25 year.

3.2 Part two

A numerical simulation is used in this section to investigate the corrosion rate at various pore saturation degrees. An appropriate numerical model requires defining boundary conditions, integrating the reaction kinetics at the steel surface, evaluating the corrosion uniformity, and solving the differential equations of transport in concrete by including the applied current density, concrete resistivity, zinc anode position, and concrete porosity [20, 32].

Ionic migration in concrete also governs the corrosion process; a relevant link exists between oxygen concentration, charge transport, and electrochemical corrosion control [33-35].

Cathodic Protection (CP) depends on multiple parameters and boundary conditions, including the concrete resistivity, anode location, concrete porosity, and characteristics of concrete components [32]. Convert the entirety of the metal surface into a cathode by applying enough current to have no electric current flowing out of the metal is one of the main methods to protect the steel surface of infrastructures either, buried or submerged; the procedure is based on two main processes sacrificial anode protection, such as zinc, or forced current protection [34].

The main difference between the two methods to enhance the steel surface resistance is the current source.

A zinc anode is implemented to investigate the steel corrosion, the potential distributions, the protection current in concrete, and the anode impact on the evolution of corrosion rate. The local current density assessment is conducted at three distinct locations on the steel surface the right side (close to the zinc anode), the point load (the applied load location), and the left side (far from the zinc anode).

3.3 Porosity and oxygen diffusivity

Concrete is considered such a multiphase porous media. In the steel/concrete interactions, the oxygen content in that interface governs the principal cathodic reaction [20].

Several investigations have shown that the increase in the dissolved oxygen level at the steel/concrete interface under diverse climatic conditions causes an extensive increase in corrosion rate [34].

The Oxygen diffusion through the porous concrete network to the steel/concrete interface has a significant impact on the corrosion process; therefore, the measurement of the oxygen diffusion coefficient is crucial.

Previous studies have demonstrated a link between diffusion/porosity and diffusion/electrical resistivity of steel-reinforced materials [3].

According to Fick's laws, the rate of oxygen diffusion is proportional to the oxygen concentration gradient.

The following equation expresses Fick's first law of diffusion:

$$\triangle.(D_i \triangle_{ci}) = R_i \tag{2}$$

$$N_i = D_i \triangle_{ci} \tag{3}$$

where: N_i: is the molar flux for i species (mol $m^{-2}s^{-1}$); D_i: is the diffusion coefficient (m^2s^{-1}); and c_i: the concentration (mol m^{-2}).

Oxygen transport through concrete is influenced by multiple factors, including pores size distribution, tortuosity, and capillary effects, as well as the concrete's moisture content, according to the governing equation for oxygen transport [20]:

$$\nabla.D_{o_2}\left(\nabla C_{o_2}\right) = 0 \tag{4}$$

where, (DO_2): is the oxygen effective diffusivity, and (∇CO_2): is the oxygen concentration gradient.

Under steady conditions, Eq. (4) must be zero for all concrete nodes in space.

3.4 Porosity and charge transport

Charge transport is a significant factor described in two different following ways in the literature. The Nernst-Planck equation, which describes charge transport based on ionic species concentration, diffusivity, and electric mobility, or using Ohm's law which relates the intensity of current (I), potential difference (V), and resistance (R) to consider concrete as a conductor, corresponding to the following equation [20, 36]:

$$I = V/R \tag{5}$$

where, the resistivity values are derived from experiments.

3.5 Modeling process

The second part of the work consists of creating a corrosion cell using numerical modeling to build a visual three-dimensional representation of the used elements; the cell is composed of the concrete as a conductive electrolyte, the steel surface of the considered RC beam, and an implemented zinc anode on the right side of the RC beam with the same porosity as the concrete. The cell voltage is controlled by a potentiostat connecting the anode and the steel surface electrically. The transport properties of ions and gases in the concrete pore network vary with the moisture content.

Concrete resistivity and oxygen-effective diffusivity values were obtained from reference [20].

The reactions considered on the steel surface are iron oxidation, water reduction (hydrogen evolution), and oxygen reduction; the oxygen and charge transport are included in the concrete electrolyte analysis.

3.6 Boundary conditions

Electrochemistry describes electrode reactions by various parameters, including thermodynamics, kinetics, and stoichiometry. The electrolytic reaction involves the exchange of electrons with the electrode and the concentrations of reactants and products at the electrolyte-electrode interface; these factors depend on the potential difference between two phases and two reactions.

The overpotential for reactions occurring at the interface is expressed as follows:

$$\eta_m = \Phi_s - \Phi_i = -E_{eq,m} \tag{6}$$

where, ϕ_s: the electric potential in the electrode; ϕ_l: the electrolyte potential; $E_{eq,m}$: the equilibrium potential.

The Tafel law related the rate of an electrochemical reaction and the overpotential [37]. The anodic Tafel's equation insertion is as follows [38]:

$$i_{loc} = i_0.10^{\frac{\eta}{A_a}} \tag{7}$$

where, A_a: Tafel slope; i_0: the current exchange density.

The cathodic Tafel expression according to the study [38] is as noted below:

$$i_{loc} = i_0.10^{\frac{\eta}{Ac}} \tag{8}$$

A_c must be negative (due to the negative sign of cathodic charge transfer reactions).

The kinetics of the Zn anode is considered to be extremely fast, and polarization is neglected in the model, setting the electrolyte potential to:

$$\Phi_{l,Zn} = -E_{eq,Zn} + \Phi_{s,Zn} = -E_{eq,Zn} \quad (9)$$

The concentration of oxygen at the Zn anode is set to atmospheric conditions as noted below:

$$C_{o_2,Zn} = C_{o\ ,ref} \quad (10)$$

Three different electrode reactions on the steel rebar boundary are considered: iron oxidation, oxygen reduction, and hydrogen evolution:

$$Fe \rightarrow Fe^{2+} + 2e^- \quad (11)$$

$$O_2 + 2H_2O + 4e^- \rightarrow 4OH^- \quad (12)$$

$$2H_2O + 2e^- \rightarrow H_2 + 2H^- \quad (13)$$

The external electric potential of the steel bar is set to -1 V, which is the applied cell potential.

The electrode kinetics of the steel bar reactions are described by Tafel expressions according to:

$$i_{Fe} = i_{0,Fe}.10^{\frac{\eta_{Fe}}{A_{Fe}}} \quad (14)$$

$$i_{O_2} = \frac{CO_2}{C_{O_2,ref}} i_{0,O_2}.10^{\frac{\eta_{O_2}}{A_{O_2}}} \quad (15)$$

$$i_{H_2} = i_{0,H_2}.10^{\frac{\eta_{H_2}}{A_{H_2}}} \quad (16)$$

η: the overpotential for each reaction is calculated as:

$$\eta = \Phi_{s,steel} - \Phi_l - E_{eq} \quad (17)$$

The electrode reaction parameters values represented in Table 1 are obtained from reference [20].

Table 1. Electrode reaction parameters values

Parameters	Unit	Zn	Fe	O_2	H_2
*E*eq	V	-0.68	-0.76	0.189	-1.03
i_0	A/m^2	-	7.1 x10^{-5}	7.7 x10^{-7}	1.1x 10^{-2}
A	V/decade	-	0.41	-0.18	-0.15

4. RESULTS AND DISCUSSION

4.1 Part one

Figure 2 represents a 3D model illustrating the overall displacement of the RC beam steel under the impact of section loss due to corrosion over ten years. The model shows that the highest deflection values are at the point load site (mid-span), where the randomly variable load is applied, which results in a maximum displacement of approximately≈35 mm.

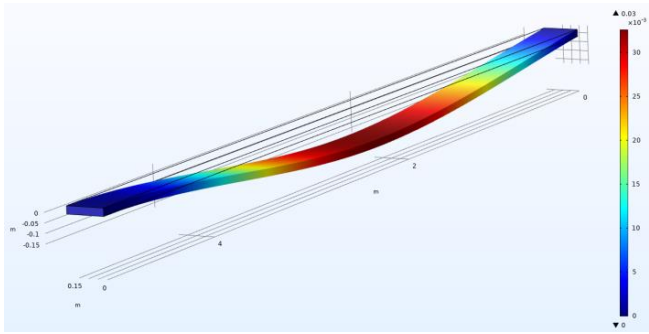

Figure 2. The total displacement of the corroded beam

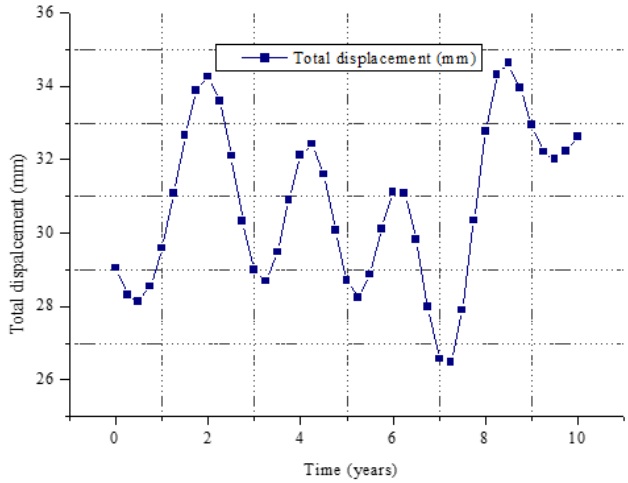

(a) Random varying loads

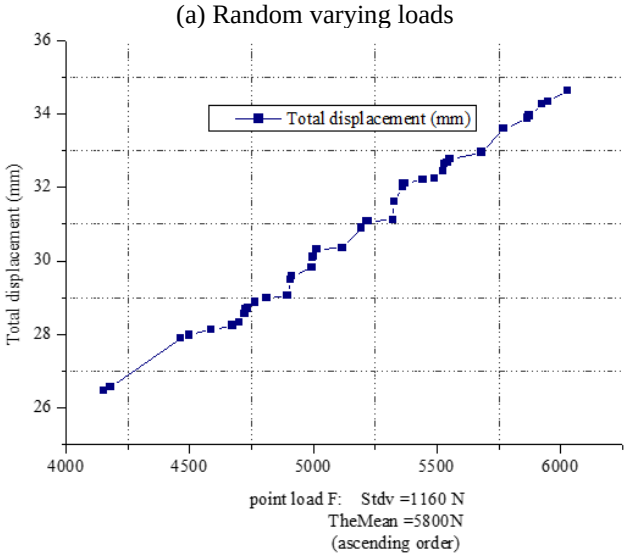

(b) Loads in ascending order

Figure 3. The total displacement of the beam under a random generated load, and section loss over a ten-years period

The beams' failure mechanism is usually in flexure; Figures 3 and 4 illustrate the displacement evolution of the studied beam model; the curves represent the beam's deflection behavior under the applied stress and the impact of corrosion degradation (sectional loss) evolving linearly during the ten years.

To create (T) the vector time: T=[0, 0.25, 0.5,0.75...10 years], the discretization of the time interval is executed into a finite number of time nodes (41 nodes), with the time discretization step Δt equal to 0.25 years.

The section loss is expressed by the corrosion coefficient c= $0.5x10^{-4}$ m /year ($0.125 x10^{-4}$ m/0.25 year).

In addition to the applied stress, the beam is subjected to its body weight ρst = 78.5 KN/m^3; the applied load vector F contains 41 values generated using the following parameters: mean μ=5800 N, and Standard deviation σ=1160 N.

The observed maximum and minimum values of the generated loads F_{Max}≈ 6028.9 N and F_{Min}≈4723.4 N resulted in a total displacement Δ_{TOT}≈0.035m and Δ_{TOT}≈0.029 m, respectively.

Figure 3 shows the total displacement of the beam under the applied stress; the deflection is plotted as a function of the applied load and time. The first case, Figure 3 (a), represents the load variation in time; it's noticeable that the interface deformation varies with the load variation at each time node. In the second case, Figure 3 (b), the load classification is in an ascending order from F_{Min} to F_{Max} to help understand the load's impact on the beam's deflection; as the stress increases, the beam's deflection increases; the graph in Figure 3 (b) illustrates better the positive correlation between the increasing load, the total beam's displacement over time, and the section loss.

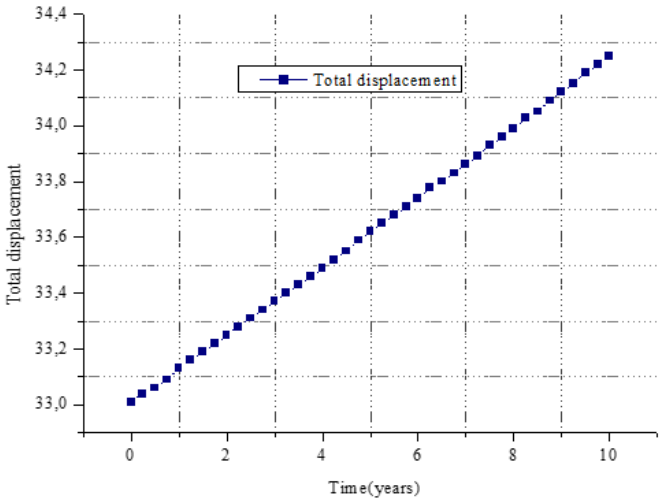

Figure 4. The total displacement of the beam under the load F=5800 N (the mean) and section loss over the ten years

To separately visualize the section loss and provide a substantial illustration of the section loss impact on the beam displacement, the load is fixed to the mean value F= 5800 N so that the beam is subjected to a single constant load F =5800 N, and isotropic corrosion evolving linearly over time with the rate of c= $0.5x10^{-4}$ m /year.

Figure 4. shows a linear increase in the total displacement over the given time frame. The results indicate a significant impact of the cross-sectional loss on the studied beam's behavior under the applied stress.

4.2 Part two

The model is solved for various pore saturation levels, using a saturation value range shifting from 20% to 80%.

The electrochemical study was conducted on three parts of the studied model: the right side of the RC beam close to the anode, the point load where the randomly generated stress is applied (the mid-span), and the left side of the beam.

The corrosion rate investigation is conducted at various pore saturation degrees of the simulated concrete pore solution. The first analysis is run for the highest pore saturation level PS=80%.

The used variable moisture range of 40% to 80% is descriptive of conditions that could be expected during drying and wetting cycles, according to Muehlenkamp et al. [20].

Figure 5 shows the impact of the implemented anode on the electrolyte potential of the simulated concrete at the highest expected pore saturation degree of 80%; the results show a noticeable lowering in the electrolyte potentials towards the right side of the RC beam.

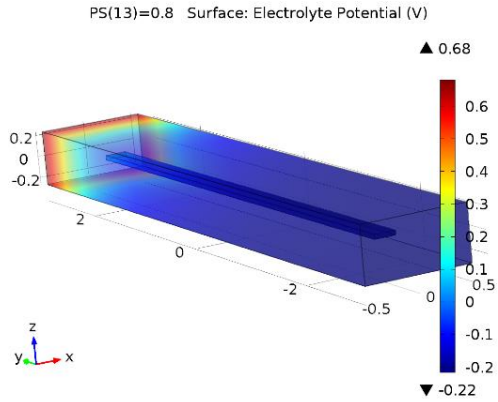

Figure 5. Electrolyte potential for an 80% pore saturation (moisture) level

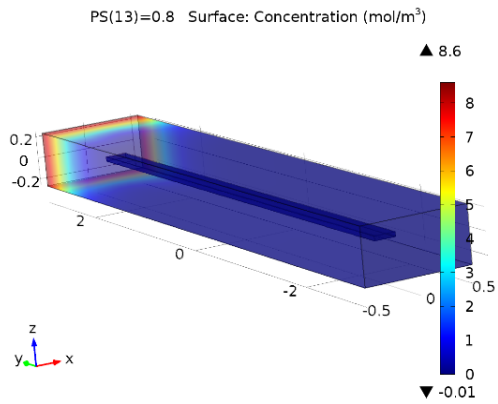

Figure 6. Oxygen concentration for an 80% pore saturation (moisture) level

In the current model analysis, the simulation of electrolyte conductivity and oxygen diffusion coefficient change as a function of concrete pore saturation.

The reaction kinetics in the steel/concrete interface, or the transport limitation, can limit the impact of mass transfer on chemical reactions rate, as in the present case, the diffusion and concrete porosity interaction problem.

Based on the three-dimensional model, Figure 6 shows oxygen concentration at a pore saturation level of the used porous material (concrete) set to 80%. A low oxygen concentration rate is noticeable all over the steel surface of the RC beam.

Because of the poor oxygen diffusion across the porous electrolyte system at high saturation degrees, oxygen hardly flows through the simulated concrete porous network,

resulting in a significant drop in the oxygen concentration level near the steel interface. From Figure 6, the results show that oxygen transport affects the system reactions limitation.

The oxygen concentration becomes negligible for higher saturation levels; the reduction kinetics must be mass transport limited as the reaction rate and the electrolyte potential are high; however, the oxygen diffusion is low, which imposes a constraint on the system's interface reactions, demonstrating the relevant link between mass transfer and surface reaction mechanisms.

The operational electrode potential characterizes the difference between the electric potentials in the corrosion cell (i.e., the difference between the potential applied by the potentiostat controlling the corrosion cell voltage and electrolyte potential).

The operating electrode potential has a significant impact on the steel beam corrosion rate; Figure 7 shows the operational electrode potential levels plotted against different values of pore saturation degrees ranging from 20, 40, 50, 60, 70, and 80% at three distinct locations on the steel surface of the RC beam (right, point load, and left).

At a saturation degree of 65%, the plotted graphs in Figure 7 show a significant decline in potential. Moreover, at the lower levels of pore saturation, a substantial potential drop can be seen for an applied cell potential of -1 V.

For a given corrosion potential, several experimental studies have shown that concrete with a low degree of saturation (i.e., dry concrete) has a higher corrosion rate than concrete with a relatively high pore saturation level (wet concrete), the higher the operating electrode potential, the lower the corrosion rate [32].

In the corrosion activation process, the presence of oxygen in the steel interface is critical; therefore, the impact of oxygen concentration variation is substantial. Figure 8 displays the local oxygen concentration at the steel interface at different degrees of saturation; a considerable concentration drop toward higher saturation levels is noticeable. The results indicate a decrease in oxygen consumption rate, causing an oxygen concentration peak at lower pore saturation levels.

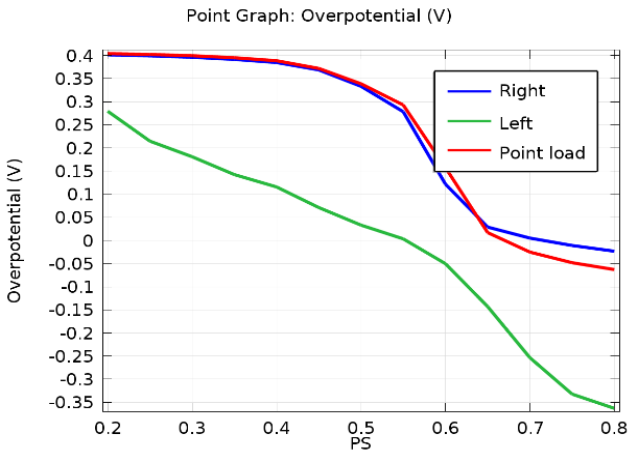

Figure 7. Operating electrode potential for three points at the RC beam electrolyte (concrete) interface

The plotted graphs in Figure 8 justify that the oxygen concentration impact on the steel corrosion in concrete, which is considered a porous electrolyte, is a function of the relevant concrete properties such as porosity and the changing moisture degrees influenced by the different surrounding environments.

The results of a combined study of oxygen concentration and pore saturation variation indicated the following: at low saturation degrees, there is a peak in oxygen concentration due to a limited rate of oxygen consumption, whereas at higher saturation levels, the oxygen diffusivity decreases due to flux limitation, resulting in a significant drop in oxygen concentration at Ps=80%, the system is constrained by oxygen transport, and the surface oxygen concentration gradually decreases up to zero.

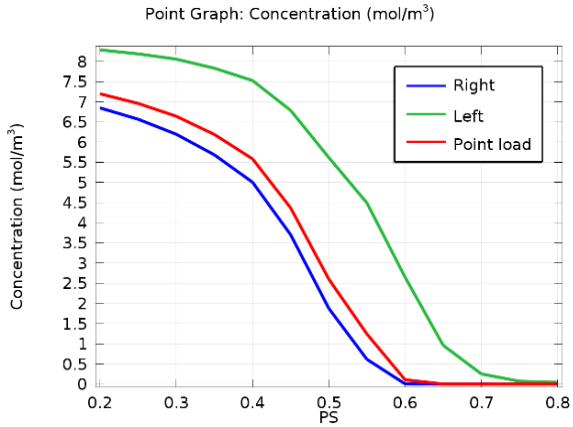

Figure 8. Local oxygen concentration at the steel-concrete interface

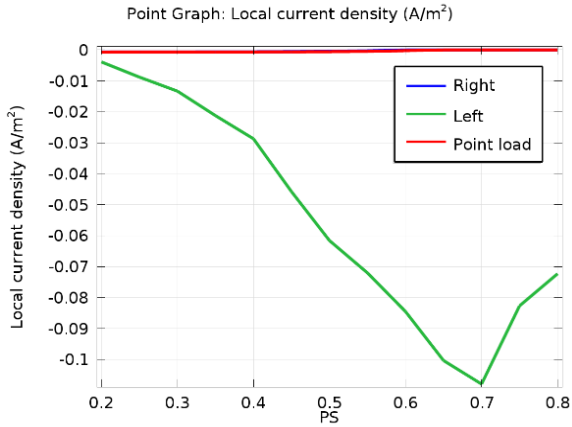

Figure 9. Local oxygen reduction current densities at the steel-concrete interface

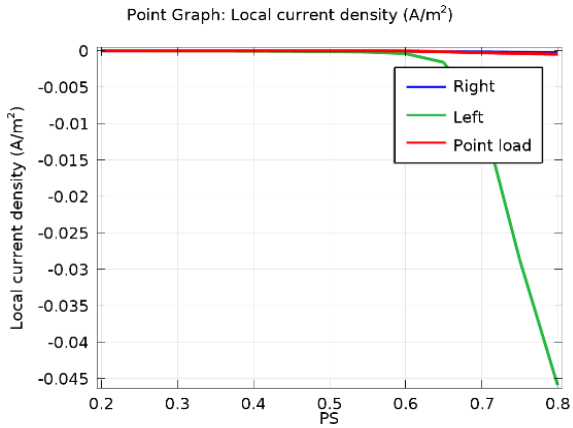

Figure 10. Local hydrogen evolution current densities at the steel -concrete interface

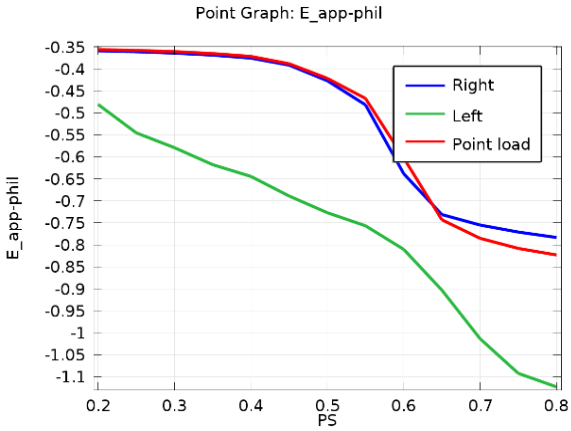

Figure 11. Iron corrosion current densities at the steel-concrete interface

Figure 9 describes the impact of saturation degrees on the oxygen reduction current density evolution for the three different considered locations of the RC beam; the graphs illustrate the proximal sides to the implemented anode (i.e., right side of the beam and point load site), indicating a certain amount of stability. The graph representing the RC beam left side in Figure 9 shows that the oxygen reduction current density magnitude is at its optimal for a Ps= 20%. In a pore saturation range varying from 20%~45%, the oxygen reduction current density is at its highest level due to the increased degree of electrolyte conductivity. At the same time, a significant drop is noticeable for a pore saturation level varying from 45%~70% due to a decrease in oxygen diffusivity in higher pore saturation levels, which reduces the current densities. Directly related to corrosion rate, the current densities increase due to an increased electrolyte conductivity until a certain point of pore saturation Ps ≈ 60%-65%; subsequently, a significant drop is noticeable for higher pore saturation levels.

Because the reduction and oxidation reactions (Red/Ox) occur evidently during the corrosion process at the steel interface, it's critical to keep track of hydrogen evolution reactions. The diffusion of hydrogen into the steel surface can alter the metal's microstructures. Figure 10 describes the hydrogen evolution current densities at the steel/concrete interface; the desorption of molecules from the cathode surface potentially limits hydrogen development. The resulting graphs plotted in Figure 10 reveal that hydrogen evolution is relatively limited below a PS level of 65% (≈0). For the hydrogen evolution reaction, 65% is the pore saturation level at which the electrode potential derived from the potential difference at the steel /concrete interface dropped below the equilibrium potential. The equilibrium is the potential where the red/ox activity of chemicals involved in the electrode reaction is equal to their concentration.

Corrosion current density variation is illustrated in Figure 11. The graphs show a significant rise in the RC beam corrosion current densities for lower saturation degrees. Whereas the steel surface undergoes a higher corrosion rate in a pore saturation range of 20%~60%, where the corrosion current densities are at their optimal values, a considerable decrease is noticeable for higher pore saturation levels of 60%~ 80%. The results demonstrated in Figure 11 confirm the pore saturation impact on oxygen mass transport resistance which decreases at high pore saturation levels, while electrical conductivity resistance increases with pore saturation.

The electrolyte conductivity and oxygen diffusion coefficient change as a function of concrete pore saturation levels, resulting in a variation of the measured corrosion rate.

At last, it is found that the electrolyte potentials are lower towards the left side of the RC beam as we get farther from the zinc anode. The magnitude of the iron oxidation current density at the steel surface is considerably smaller than the oxygen reduction and hydrogen evolution current densities, which demonstrate the impact of the added zinc anode on the right side of the beam as cathodic protection on the corrosion rate evolution.

5. CONCLUSIONS

The importance of mechano-electrochemical coupling techniques is demonstrated in this study using numerical modeling. The work is structured in two sections; the found results lead to the following conclusions:

1. Section loss can characterize corrosion degree in practice. The steel sectional isotropic reduction due to corrosion has a critical impact on the total displacement, which affects the functionality of the structure's elements over time.
2. There is a positive correlation between the total displacement and load variation. The beam's deflection increases over time as the steel's section decreases.
3. As the corrosion degree increases, the RC beam's yield strength and ultimate strength deteriorate due to the steel's section reduction, which reduces the corroded steel element ductility.
4. The pore saturation degree of the simulated concrete principally governs the corrosion rate; the degree of corrosion uniformity is controlled by the concrete's relative humidity in the proximity of the steel surface.
5. In the steel/concrete interface proximity, the oxygen concentration becomes negligible for higher pore saturation levels, demonstrating the low flux of oxygen into the RC beam's steel interface due to the decrease in oxygen diffusivity.
6. For a given corrosion potential, dry conditions (low concrete saturation degrees) have higher corrosion rates than wet conditions (high concrete pore saturation degrees).
7. It's crucial to keep track of hydrogen evolution reactions; the hydrogen diffusion into the steel surface can alter the metal's microstructures. In low pore saturation conditions, hydrogen evolution is relatively limited, and the desorption of molecules from the cathode surface could limit hydrogen production.
8. The operating electrode potential is a significant determinant in the corrosion rate evaluation; at a given corrosion potential, concrete with a low saturation degree undergoes a higher corrosion rate than concrete with a higher pore saturation level.
9. A considerable decrease in corrosion rate is noticed for higher pore saturation levels, confirming the impact of pore saturation on oxygen mass transport resistance, which decreases at high pore saturation levels while electrical conductivity resistance increases.
10. The efficiency of the implemented zinc anode in the corrosion protection of the RC beam's steel surface demonstrates the importance of the zinc coating protection method in steel rebar corrosion prevention. It's found that the anode impact differs in function of both the position on the RC beam and the concrete moisture content.

The corroded steel assessment in a porous simulated media (concrete) under different pore saturation levels will help predict the behavior of corroded elements subjected to time-varying loading in harsh environmental conditions.

The coupled numerical modeling of the mechanical and electrochemical impact of corrosion on RC elements demonstrates the chemical corrosion reactions' impact on the mechanical behavior of reinforced steel infrastructures. This study provides a substantial perception of the electrochemical reactions involved in corrosion processes, combined with the mechanical effect of structure loading.

In this work, we define the fundamental problem of the corrosion mechanism and its complexity in RC structures under multiple conditions, varying the pore saturation degree of the used electrolyte under alternating loading, including cathodic protection. The analysis in this study is conducted completely using numerical simulations. The study seems challenging due to limited access to experiments data for this purpose, the electrode reaction parameter values used in part 2 were obtained from the reference [20]. This subject can be examined further by including additional parameters like temperature and other corrosion prevention techniques to understand the corroded RC structures' behavior better. Much research also remains to be done on this topic.

ACKNOWLEDGMENT

The authors gratefully acknowledge Elsevier for the permission to reuse some data/material.

REFERENCES

[1] Marcus, P., Mansfeld, F.B. (2006). Analytical Methods in Corrosion Science and Engeneering. CRC Press. https://doi.org/10.1201/9781420028331

[2] Yuan, J., Zhao, B., Wang, Z., Liu, Y. (2020). Carbonization law of fly ash concrete under freeze-thaw cycles based on image-pro plus. Annales de Chimie-Science des Matériaux, 44(6): 393-398. https://doi.org/10.18280/ACSM.440604

[3] Linares-Alemparte, P., Andrade, C., Baza, D. (2019). Porosity and electrical resistivity-based empirical calculation of the oxygen diffusion coefficient in concrete. Construction and Building Materials, 198: 710-717. https://doi.org/10.1016/j.conbuildmat.2018.11.269

[4] Durga, C.S.S., Ruben, N. (2019). Assessment of various self healing materials to enhance the durability of concrete structures. Annales de Chimie-Science des Matériaux, 43(2): 75-79. https://doi.org/10.18280/acsm.430202

[5] Khemissa, M., Tallah, N., Bencheikh, B. (2018). Experimental and numerical modeling of the sand–steel interface behavior under monotonic loading. Innovative Infrastructure Solutions, 3(1): 1-10. https://doi.org/10.1007/s41062-018-0130-y

[6] Van Der Giessen, E., Schultz, P.A., Bertin, N., Bulatov, V.V., Cai, W., Csányi, G., Tadmor, E.B. (2020). Roadmap on multiscale materials modeling. Modelling and Simulation in Materials Science and Engineering, 28(4): 043001. https://doi.org/10.1088/1361-651X/ab7150

[7] Fujimoto, S. (2014). Numerical modeling for corrosion. Electrochemical Society Interface, 23: 45. https://doi.org/10.1149/2.F01144IF

[8] Chen, Y., Huang, H., Zhang, Y., Wang, C., Fan, W. (2018). A method of atmospheric corrosion prediction for aircraft structure. Materials and Corrosion, 70: 79-90. https://doi.org/10.1002/maco.201810391

[9] Liu, C., Kelly, R.G. (2014). The use of finite element methods (FEM) in the modeling of localized corrosion. Electrochemical Society Interface, 23: 47-51. https://doi.org/10.1149/2.F02144IF

[10] Kobidze, G., Lord, W., Udpa, S. (1998). Integrating a stress corrosion crack model into finite element electromagnetic NDT code. Review of Progress in Quantitative Nondestructive Evaluation, 17: 323-330. https://doi.org/10.1007/978-1-4615-5339-7_41

[11] Taylor, C.D. (2015). Corrosion informatics: An integrated approach to modelling corrosion. Corrosion Engineering, Science and Technology, 50: 490-508. https://doi.org/10.1179/1743278215Y.0000000012

[12] Gutman, E.M. (1994). Mechanochemistry of Solid Surfaces. World Scientific Publication Singapore. https://doi.org/10.1142/2373

[13] Bogdanov, R.I., Unigovski, Y.B., Gutman, E.M., Ryakhovskikh, I.V., Shneck, R.Z. (2019). Stress corrosion cracking of pipeline steels in near-neutral pH solutions: The role of mechanochemical and chemomechanical effects. AIMS Materials Science, 6: 1065-1085. https://doi.org/10.3934/MATERSCI.2019.6.1065

[14] Li, B., Fang, H., He, H., Yang, K., Chen, C., Wang, F. (2019). Numerical simulation and full-scale test on dynamic response of corroded concrete pipelines under Multi-field coupling. Construction and Building Materials, 200: 368-386. https://doi.org/10.1016/j.conbuildmat.2018.12.111

[15] Xu, L.Y., Cheng, Y.F. (2013). Development of a finite element model for simulation and prediction of mechanoelectrochemical effect of pipeline corrosion. Corrosion Science, 73: 150-160. https://doi.org/10.1016/j.corsci.2013.04.004

[16] Xu, L.Y., Cheng, Y.F. (2012). Corrosion of X100 pipeline steel under plastic strain in a neutral pH bicarbonate solution. Corrosion Science, 59: 103-109. https://doi.org/10.1016/j.corsci.2012.02.022

[17] Xu, L.Y., Cheng, Y.F. (2012). Reliability and failure pressure prediction of various grades of pipeline steel in the presence of corrosion defects and pre-strain. International Journal of Pressure Vessels and Piping, 89: 75-84. https://doi.org/10.1016/j.ijpvp.2011.09.008

[18] Andrade, C.U., Alonso, C. (2001). On-site measurements of corrosion rate of reinforcements. Construction and Building Materials, 15: 141-145. https://doi.org/10.1016/S0950-0618(00)00063-5

[19] Koushik, B.G., Van den Steen, N., Mamme, M.H., Van Ingelgem, Y., Terryn, H. (2020). Review on modelling of corrosion under droplet electrolyte for predicting atmospheric corrosion rate. Journal of Materials Science & Technology, 62: 254-267. https://doi.org/10.1016/j.jmst.2020.04.061

[20] Muehlenkamp, E.B., Koretsky, M.D., Westall, J.C. (2005). Effect of moisture on the spatial uniformity of cathodic protection of steel in reinforced concrete. Corrosion, 61: 519-533. https://doi.org/10.5006/1.3278188

[21] Jašniok, T., Jašniok, M. (2015). Influence of rapid changes of moisture content in concrete and temperature on corrosion rate of reinforcing steel. Procedia Engineering, 108: 316-323. https://doi.org/10.1016/j.proeng.2015.06.153
[22] Chen, L., Su, R.K.L. (2020). Corrosion rate measurement by using polarization resistance method for microcell and macrocell corrosion: Theoretical analysis and experimental work with simulated concrete pore solution. Construction and Building Materials, 121003. https://doi.org/10.1016/j.conbuildmat.2020.121003
[23] Nasser, H., Steen, C.V.A.N., Vrijdaghs, R., Torres, A.A., Vandewalle, L., Erstrynge, E. (2019). Numerical modelling of corroded reinforced concrete beams based on visual inspection data. SMAR 2019 the fifth conference on Smart Monitoring Assessment and Rehabilitation of Civil Structures, pp. 1-8.
[24] Azoor, R.M., Deo, R.N., Birbilis, N., Kodikara, J. (2019). On the optimum soil moisture for underground corrosion in different soil types. Corrosion Science, 159: 108-116. https://doi.org/10.1016/j.corsci.2019.108116
[25] Hirata, R., Ooi, A., Tada, E., Nishikata, A. (2021). Influence of the degree of saturation on carbon steel corrosion in soil. Corrosion Science, 189: 109568. https://doi.org/10.1016/j.corsci.2021.1095681.109568
[26] Andrieu-Renaud, C., Sudret, B., Lemaire, M. (2004). The PHI2 method: A way to compute time-variant reliability. Reliability Engineering & System Safety, 84(1): 75-86. https://doi.org/10.1016/j.ress.2003.10.005
[27] Xu, L., Cheng, Y.F. (2017). A finite element based model for prediction of corrosion defect growth on pipelines. International Journal of Pressure Vessels and Piping, 153: 70-79. http://dx.doi.org/10.1016/j.ijpvp.2017.05.002
[28] Chen, J., Zhang, W., Gu, X. (2019). Modeling time-dependent circumferential non-uniform corrosion of steel bars in concrete considering corrosion-induced cracking effects. Engineering Structures, 201: 109766. https://doi.org/10.1016/j.engstruct.2019.109766
[29] Kabashi, N., Avdyli, B., Krasniqi, E., Këpuska, A. (2020). Comparative approach to flexural behavior of reinforced beams with GFRP, CFRP, and steel bars. Civil Engineering Journal, 6: 50-59. https://doi.org/10.1051/e3sconf/201913101031
[30] Wang, K., Li, C., Li, Y., Lu, J., Wang, Y., Luo, X. (2020). A fully coupled model of hydrodynamic-chemical-electrochemical processes for CO_2 uniform corrosion in multi-physics environment. Journal of Petroleum Science and Engineering, 193: 107-436. https://doi.org/10.1016/j.petrol.2020.107436
[31] Yu, Y., Gao, W., Castel, A., Liu, A., Feng, Y., Chen, X. (2020). Cement and concrete research modelling steel corrosion under concrete non-uniformity and structural defects. Cement and Concrete Research, 135: 106-109. https://doi.org/10.1016/j.cemconres.2020.106109
[32] Goyal, A., Olorunnipa, E.K., Pouya, H.S., Ganjian, E., Olubanwo, A.O. (2020). Potential and current distribution across different layers of reinforcement in reinforced concrete cathodic protection system- A numerical study. Construction and Building Materials, 262: 120-580. https://doi.org/10.1016/j.conbuildmat.2020.120580
[33] Asselin, E., Alfantazi, A., Rogak, S. (2007). Effect of oxygen on the corrosion behavior of alloy 625 from 25 to 200℃. Journal of The Electrochemical Society, 154: C215. https://doi.org/10.1149/1.2435620
[34] Yan, X., Wang, Y., Du, Q., Jiang, W., Shang, F., Li, R. (2019). Research progress on factors affecting oxygen corrosion and countermeasures in oilfield development. E3S Web Conf 131. https://doi.org/10.1051/e3sconf/201913101031
[35] Hussain, R., Ishida, T., Wasim, M. (2012). Oxygen transport and corrosion of steel in concrete under varying concrete cover, w/c, and moisture. ACI Materials Journal, 109: 3-10. https://doi.org/ 14359/51683565
[36] Luchetti, M. (2020). From successful measurement to the birth of a law: Disentangling coordination in Ohm's scientific practice. Studies in History and Philosophy of Science Part A, 84: 119-131. https://doi.org/10.1016/j.shpsa.2020.09.005
[37] Allen, L.R.F., Bard, J. (2000). Electrochemical Methods: Fundamentals and Applications, 2nd Edition.
[38] COMSOL. (2003). Electrochemistry module User's Guide. Mater. Today, 6(9): 107-113.

NOMENCLATURE

I	The intensity of the current, A
V	Potential difference, V
R	The resistance, Ω
A_{Fe}	Tafel slope iron oxidation
A_{H2}	Tafel slope hydrogen evolution
A_{O2}	Tafel slope oxygen reduction
$C_{O2,ref}$	Oxygen reference concentration
$i_{0,Fe}$	Iron oxidation exchange current density, A/m^2
$i_{0,H2}$	Hydrogen evolution current density, A/m^2
$i_{0,O2}$	Oxygen reduction exchange current density, A/m^2
$E_{eq,Zn}$	Zn equilibrium potential, V
$C_{O2,Zn}$	the oxygen concentration at the concrete-zinc interface
Eeq	Equilibrium potential, V

Greek symbols

ϕ_l	electric potential in concrete, V
$\phi_{s,steel}$	The external electric potential of the steel beam, V
$\phi_{s,Zn}$	Potential of steel at Zn anode-concrete interface, V
$\phi_{l,Zn}$	electrolyte potential, at Zn anode-concrete interface, V
∇	Gradient operator
η	the overpotential, V

Subscripts

D_i	diffusion coefficient
N_i	molar flux for i species